Available online at www.sciencedirect.com

SCIENCE DIRECT®

Clinical Biomechanics 20 (2005) 998–1006

CLINICAL BIOMECHANICS

www.elsevier.com/locate/clinbiomech

Delay of intracortical bone remodelling following a stress change: A theoretical and experimental study

Alexandre Terrier [a,*], Junpei Miyagaki [b], Hiromichi Fujie [b], Kozaburo Hayashi [b], Lalao Rakotomanana [c]

[a] *Laboratoire de Recherche en Orthopédie, Ecole Polytechnique Fédérale, de Lausanne (EPFL), 1015 Lausanne, Switzerland*
[b] *Division of Mechanical Science, Graduate School of Engineering Science, Osaka University, Toyonaka, Osaka 560-8531, Japan*
[c] *Institut de Recherche Mathématique de Rennes, UMR 6625 du CNRS 35042, Rennes cedex, France*

Received 21 September 2004; accepted 15 June 2005

Abstract

Background. A theoretical model and an experimental setup were specifically designed to identify and determine the delay of the cortical bone response (restricted to mineralization and demineralization) to a stress change.

Methods. The in vivo experiment considered two groups of rats: a running group and a control sedentary group. The running group rats were compelled to a running activity for 15 weeks, followed by a sedentary activity for 15 weeks. Bone density was derived from hardness measurements. The parameters of the remodelling theory, including the response delay and the remodelling rates, were determined from these experimental measurements.

Findings. Bone density increased significantly during the activity period, and decreased rapidly when rats returned to sedentary state. The identification of the model's parameters produced evolution curves that were within the limits of the standard deviation of the experimental data. The densification rate was lower than the resorption rate, and the densification delay was greater than bone resorption delay.

Interpretation. The delays determined with this macroscopic model are related to response delays due to biological internal processes in bone.

Keywords: Bone; Remodelling; Adaptation; Rat

1. Introduction

Living bone has the ability to adapt its properties to the change of mechanical load environment. An augmentation of physical activities such as running significantly increases the bone formation and mineralization (Bourrin et al., 1995; Eliakim et al., 1997) whereas a long-term disuse of the skeleton involves inhibition of bone formation and induces significant demineralization of bone (Kaneps et al., 1997; Vico et al., 1998). The effects of training and detraining have therefore been studied by numerous authors. For rat models, relative short period of six weeks of remobilization following six weeks of hindlimb immobilization resulted in incomplete recovery of bone mass (Maeda et al., 1993). Longer period of 18 weeks of hindlimb immobilization followed by 20 weeks of remobilization resulted in a 34% decrease of trabecular bone area of distal tibiae. Dog models have been used to show complete recovery of bone mass following immobilization, but combined with exercise (Kaneps et al., 1997). To date, although mechanical loading is an important factor in the bone tissue maintenance, the type and magnitude of exercises used and

* Corresponding author.
E-mail address: alexandre.terrier@epfl.ch (A. Terrier).

0268-0033/$ - see front matter © 2005 Elsevier Ltd. All rights reserved.
doi:10.1016/j.clinbiomech.2005.06.008

how long it is most effectively prescribed are still inconclusive (Bennell et al., 2000). The main reason is that the interpretation of these in vivo results remains difficult since many factors are involved in the adaptation of bone to a stress change: like the stimulus to consider, other biological factors, genetic, aging factors, etc. Among these factors, the time delay between the stress change and the bone response is certainly important.

Experiments on rats have shown that weightlessness does not change bone mass in the early phase of a spaceflight (Vico et al., 1998). Following an immobilization of the lower limb after a fracture of the human tibia, the densification process caused by remobilization was only observed several weeks after the remobilization started (Ulivieri et al., 1990). Conversely, rat experiments pointed out that the rate of bone formation increased significantly in weeks 3–5 only after the physical exercise started (Bourrin et al., 1995). In the same way, after 10 weeks of training, previous studies have shown that after stopping the running exercise, the training effects remain and cortical bone increase do not diminish immediately after cessation of training (Kiuchi et al., 1998). Numerous macroscopic models of bone remodelling have then been developed for simulating and interpreting the long-term bone reaction to change of physical activities and after orthopaedic surgery (e.g., Cowin, 1986; Terrier et al., 1997a,b). In these models, the mechanical stimulus is proportional to an effective stress measure, which accounts for the various loading conditions. However, the delay of bone response was rarely introduced in bone adaptation models (Levenston et al., 1994; Terrier et al., 1997a,b; Hazelwood et al., 2001). As far as we know, the parameters of the intracortical bone remodelling, such as the delays of resorption (decrease of the mineralized tissue) and formation (increase of the mineralized tissue) were not experimentally determined despite the sophistication of the most recent models.

Therefore, the purpose of the present study was to determine the parameters of a bone adaptation model from experimental data. The theoretical model was specially developed to account for the delay between stress change and intracortical bone response, and the experiment protocol was also specifically design to measure this delay.

2. Theory

2.1. Experimental observations on bone tissue

There are two types of bone tissues: cortical and spongious. Cortical bone is a dense material. Bone external surface is called periostal surface. The interior surface is called endosteal surface. From microscopic point of view, there are three types of cortical bone: woven, laminar, and harvesian. Woven bone is found in young humans and young animals and also in adults after some bone injury. During normal maturation, it is gradually replaced by laminar bone. Generally, laminar bone consists of number of concentrically arranged laminae (about 10–20 mm long). Harvesian bone is organized to accommodate small arteries, arterioles, capillaries and venules of microcirculating system. The osteons of harvesian bone and the laminae of laminar bone are basically just different geometrical configurations of the same material. The interface between laminae have an ellipsoidal form which contain bone cells. Cortical bone is blood supplied. Cancellous bone is composed of short struts of bone material (trabeculae). The connected trabeculae give cancellous bone a spongy appearance. There are no blood vessels within the trabeculae but there are vessels immediately adjacent to the tissue. The density of cortical bone is its mass per unit volume. The density of human cortical bone ranges from about 1.7 g/cm^3 to 2.0 g/cm^3. Two densities can be measured for the cancellous bone: the density of the trabecular bone material and the density of trabecular structure. The density of the trabecular material ranges from 1.6 g/cm^3 to 1.9 g/cm^3. The density of the trabecular structure ranges from 0.15 g/cm^3 to 0.7 g/cm^3.

2.2. Continuum model of bone tissue

The non-homogeneity of bone was described by the relative density ρ, defined by

$$\phi = \frac{\rho}{\rho_{\mathrm{m}}}, \tag{1}$$

where ρ_{m} is the density of the fully mineralized tissue and ρ the bone apparent density, which is the ratio of mineralized tissue mass on the total tissue volume ($0 \leqslant \phi \leqslant 1$). Cortical bone was assumed to have transversely isotropic symmetry, entirely characterized by a unit vector $\mathbf{v}$ representing the anisotropy direction, which might vary in the material. Indeed, for transversely isotropic material, the structural tensor $\mathbf{M} \equiv \mathbf{v} \otimes \mathbf{v}$ is sufficient to describe the material symmetry. For modelling dissipative process within the bone, we shall assume that bone state is determined by a set of variables, which consists in the strain $\mathbf{C}$, the relative density ϕ and the structural tensor $\mathbf{M}$. Unlike the strain $\mathbf{C}$, the structural variables ϕ and $\mathbf{M}$ are internal variables, which do not explicitly appear in the conservation laws: mass, linear momentum, angular momentum, energy. In the case of uniform and constant temperature fields, the entropy inequality reduced to

$$\left(\mathbf{S} - 2\rho_0 \frac{\partial \xi}{\partial \mathbf{C}}\right) : \frac{\dot{\mathbf{C}}}{2} - \rho_0 \frac{\partial \xi}{\partial \phi}\dot{\phi} - \rho_0 \frac{\partial \xi}{\partial \mathbf{M}}\dot{\mathbf{M}} \geqslant 0, \tag{2}$$

where $\mathbf{S}$ is the second tensor of Piola–Kirshoff, ρ_0 the density in the initial configuration, and $\xi = \xi(\mathbf{C}, \phi, \mathbf{M})$

the Helmoltz free energy. The characteristic time of the adaptation process is about one week. It is much greater than the characteristic time of the global external load change (about 1 h), caused by common activity like standing, running or walking. The latter is also much greater than the characteristic time of the cyclic stress found in daily activities (about one second). Hence, the remodelling phenomenon is related to a mechanical process that has a very different time scale. Therefore, a time-homogenization is performed by neglecting the time derivatives $\dot{\phi}$ and $\dot{\mathbf{M}}$ in front of $\dot{\mathbf{C}}$, and it is thus reasonable to assume that the stress is not caused by a change of internal structure, but only by deformation. Deducted from a continuum model based on a quadratic free energy (e.g., Rakotomanana, 2004), the bone tissue constitutive law takes the form of

$$\mathbf{S} = [e_1 \operatorname{Tr}\mathbf{E} + e_4 \operatorname{Tr}(\mathbf{ME})]\mathbf{I} + e_2\mathbf{E} + [e_3 \operatorname{Tr}\mathbf{E} + e_5 \operatorname{Tr}(\mathbf{ME})]\mathbf{M} + e_4[\mathbf{ME} + \mathbf{EM}], \tag{3}$$

where $\mathbf{E} \equiv \frac{1}{2}(\mathbf{C} - \mathbf{I})$ is the Green–Lagrange strain tensor and e_i $(i = \overline{1,5})$ are the elastic coefficients of the bone tissue assumed to have transverse isotropic symmetry. It is worthwhile to notice that $e_i = e_i(\phi)$. Based on in vitro experimental measurements, this dependence is usually assumed quadratic (Cowin, 1989).

2.3. Mechanical stimulus of remodelling

The keystone of a bone adaptation model is the choice of the stimulus function ψ, which was here a function of the mineralized bone density ϕ, the anisotropy $\mathbf{M}$ and the stress $\mathbf{S}$, depending therefore on the isotropic and anisotropic stress modes. Following the hypothesis that intracortical bone remodelling serves to repair microcracks (Kummer, 1972), and since the production and amount of microcracks within cortical bone can be related to the damage, the anisotropic yield stress criterion of Hill, designated thereafter by Y, was chosen as a base for the stimulus function (Zioupos et al., 1995). It depends on the stress $\mathbf{S}$, but also on the relative density ϕ through five anisotropic plastic coefficients (Rubin et al., 1993; Rakotomanana et al., 1999). This quantity includes all stress modes, such as compression/traction due to axial loading, and shearing stress due to torsional loading (Rakotomanana et al., 1992). Instead of conventional stress tensor invariants, physical invariants were introduced: hydrostatic pressure p, octahedral shear stress τ_{oct}, longitudinal stress acting along the privileged direction of anisotropy σ_{nn} and shear stress perpendicular to this privileged direction τ_{vv} (Rakotomanana et al., 1999):

$$p \equiv \tfrac{1}{3}\operatorname{Tr}\mathbf{S}, \quad \tau_{\text{oct}} \equiv \sqrt{\operatorname{Tr}\mathbf{S}^2 - \tfrac{1}{3}(\operatorname{Tr}\mathbf{S})^2}, \qquad \sigma_{vv} \equiv \operatorname{Tr}\mathbf{MS}, \quad \tau_{vv} \equiv \sqrt{\operatorname{Tr}\mathbf{MS}^2 - \tfrac{1}{3}(\operatorname{Tr}\mathbf{MS})^2}. \tag{4}$$

As a simplified assumption and conforming to classical theories of plasticity, we only retain quadratic terms for the plastic yield stress and thus for the remodelling stimulus. Therefore, the most general expression of a quadratic remodelling mechanical stimulus (based on stress and accounting for transverse anisotropy) takes the form of

$$Y(\phi, \mathbf{M}, \mathbf{S}) = R_1 p + R_2\sigma_{vv} + R_3 p\sigma_{vv} + R_4 p^2 + R_5\tau_{\text{oct}} + R_6\tau_{vv}^2 + R_7\sigma_{vv}^2, \tag{5}$$

which constitutes an extension of the von Mises plastic yield stress function for transverse isotropic material. The remodelling functions R_i are functions of the plastic coefficients p_i (cf. Hill criterion) as follows:

$$R_1 = R_2 = 0, \quad R_3 = 3p_3, \quad R_4 = \tfrac{9}{2}p_1 + \tfrac{3}{2}p_2, \quad R_5 = \tfrac{1}{2}p_2, \quad R_6 = p_4, \quad R_7 = p_4 + \tfrac{1}{2}p_5, \tag{6}$$

where linear functions R_1 and R_2 are excluded, and where the plastic coefficients p_i are shown to be functions of the relative density ϕ through the stress strengths σ_{ij} (Rakotomanana et al., 1992, 1999):

$$p_1 = -\frac{2}{\sigma_1^2} + \frac{1}{\sigma_3^2}, \quad p_2 = \frac{1}{\sigma_{12}^2}, \quad p_3 = \frac{2}{\sigma_1^2} - \frac{2}{\sigma_3^2}, \quad p_4 = \frac{1}{\sigma_{13}^2} - \frac{1}{\sigma_{12}^2}, \quad p_5 = \frac{2}{\sigma_1^2} + \frac{4}{\sigma_3^2} - \frac{2}{\sigma_{13}^2}. \tag{7}$$

According to the expression of Y, we recovered different models of mechanical stimuli (based on stress) proposed in the literature (Terrier et al., 1997a,b). Experimental studies have shown that the stress strengths σ_{ij} are correlated to the relative density ϕ according to

$$\sigma_{ij}(\phi) = \sigma_{ijc}\phi^2, \tag{8}$$

where σ_{ijc} correspond to cortical bone stress strengths.

2.4. Time evolution of remodelling

For the sake of simplicity, we focused on the intracortical bone remodelling in the tibial shaft of young growing rats. Indeed, the tibial shaft is one of the bone site well adapted for experimental measurements since it is a load bearing bone (Iwamoto et al., 1999). Since the average orientation of the mineralized collagen fibre in the tibia diaphysis is approximately parallel to the bone's long axis, cortical bone tissue was assumed to have transversely isotropic symmetry. The privileged axis of anisotropy $\mathbf{v}$ was directed along the tibial axis, and not modified by the remodelling process. Non-homogeneous properties of bone were described through the relative density ϕ. The intracortical adaptation model related the rate of relative density ϕ to the mechanical stimulus ψ by a piece-wise linear relation (Beaupre et al., 1990):

$$\frac{d\phi}{dt} = \begin{cases} v_r(\psi - \psi_r), & \psi < \psi_r, \\ 0, & \psi_r < \psi < \psi_d, \\ v_d(\psi - \psi_d), & \psi_d < \psi, \end{cases} \quad (9)$$

where v_r and v_d were, respectively, the resorption and densification rates. When ψ was within the equilibrium zone $[\psi_r, \psi_d]$ the remodelling rate was zero (Fig. 1). The remodelling stimulus ψ, which was based on the function Y, not only included the present value of Y, but its whole history. This stress history and the delay between stress change and bone response was introduced by an integral operator, weighted by an exponential fading memory function (Terrier et al., 1997a,b):

$$\psi(t) = \int_{-\infty}^{t} Y(S) \frac{1}{\tau} \exp\left(-\frac{t-s}{\tau}\right) ds, \quad (10)$$

where a specific delay parameter τ was introduced for resorption (τ_r) and for densification (τ_d). For numerical simulations as in finite element methods, it was convenient to transform the integro-differential equations by changing variables $s' \equiv t - s$ and by integrating by parts:

$$\frac{d\psi}{dt} = \left[-Y(t-s')\frac{1}{\tau}\exp\left(-\frac{s'}{\tau}\right)\right]_0^{\infty} + \int_0^{\infty} Y(t-s')\left(-\frac{1}{\tau^2}\right)\exp\left(-\frac{s'}{\tau}\right) ds', \quad (11)$$

to get the following system of differential equations:

$$\begin{cases} \frac{d\phi}{dt} = v_\alpha[\psi(t) - \psi_\alpha], \\ \frac{d\psi}{dt} = \frac{1}{\tau}\left[\frac{\widetilde{Y}(t)}{\phi^4} - \psi(t)\right], \end{cases} \quad (12)$$

with the initial conditions $\phi(0) = \phi_0$ and $\psi(0) = \psi_0$, and where $\alpha = r$ if $\psi < \psi_r$, $\alpha = d$ if $\psi > \psi_d$, $v_\alpha = 0$ if $\psi_r < \psi < \psi_d$, and where $\widetilde{Y} = Y\phi^4$ (Terrier et al., 1997a,b).

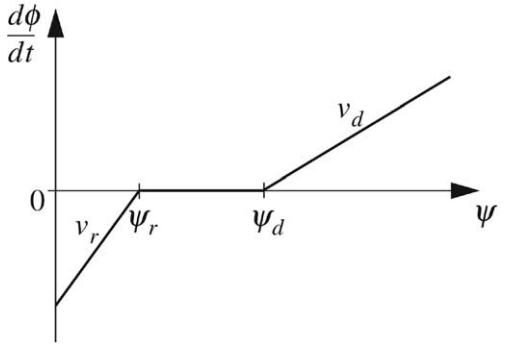

Fig. 1. Intracortical adaptation law defined by a piece-wise linear relationship between the rate of relative density and the mechanical stimulus. Within the equilibrium zone (between ψ_r and ψ_d), no adaptation occurs. Outside, the resorption and densification rates are characterized by v_r and v_d.

3. Experiment

Eighty female Wistar rats (nine-week-old) were randomly divided into a control and a running group (all animal experiments were conducted at Osaka University, under the Guidelines of the Committee for Animal Care and Use of the University). The rats of the running group were subjected to a daily running program for 15 weeks: one hour running per day, six days per week on a motor-driven treadmill. On the first day, the treadmill speed was set to 1.2 km/h; it was gradually increased during the following four days to 1.6 km/h, and then maintained for the remainder of the running period. After this running period, the rats of the running group were returned to normal activity (sedentary state in cages) for 15 weeks, called thereafter the control period. The rats of the control group were subjected to sedentary state in cages during the whole experiment period (Fujie et al., 2004). At week 0, 3, 7, 15 (end of running period), 16, 18, 22, and 30 (end of experiment), five rats of each group were sacrificed. Hardness (micro-Vickers) measurements (MVK-G1, AKASHI, Yokohama, Japan) were carried out on a transversal surface, precisely located in the midshaft of the left tibia, in four main regions: anterior (A), posterior (P), medial (M), and lateral (L). In each of these regions, five measurements were made near the endost (100 μm from the internal surface), near the periosteum (150 μm from the external surface) and in the middle of these two locations (Fig. 2).

Thereafter only mean hardness values were considered. The average was based on 300 hardness measurements (60 measurements × 5 rats). For the identification process, these mean hardness values were correlated to relative density ϕ according to the following procedure. During the running period, the mean bone hardness of the running group H_r progressively increased, and was significantly different from the one of the control group H_c at the end of this period. During the second period, it returned to a value slightly above the control. The control group also displayed an increase of hardness during the experiment period (Fig. 3, left). However, this hardness increase was caused by natural growth, since the rats were not skeletally mature at the start of the experiment. In order to remove this growth effect, which was presumably equally present in the running group, and thus to isolate the effect of adaptation caused by the running activity, the hardness measurements needed to be transformed. For this purpose, a linear curve $\overline{H}(t_i)$ was fit to the control group hardness $H_c(t_i)$, and then subtracted from the running group hardness $H_r(t_i)$. This hardness difference $\Delta H(t_i)$ was thus attributed to the running activity effect. In order that the final transformed hardness of the control $\widetilde{H}_c(t_i)$ and running $\widetilde{H}_r(t_i)$ group led in a physiological range, a reference hardness value $\overline{H}(t = 15 \text{ weeks})$ was

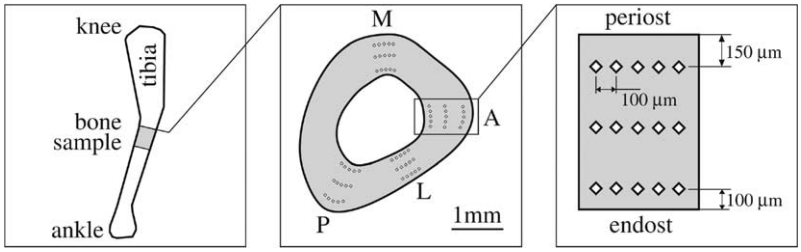

Fig. 2. Location of the hardness measurements: transversal surfaces of the midshaft of the left tibia, in four main regions: anterior (A), posterior (P), medial (M) and lateral (L). In each region, five measurements were performed at the periosteum, endosteum and in the middle of the cortical bone, respectively. The grey zone in the left figure shows the location of the bone sample used for the compression tests.

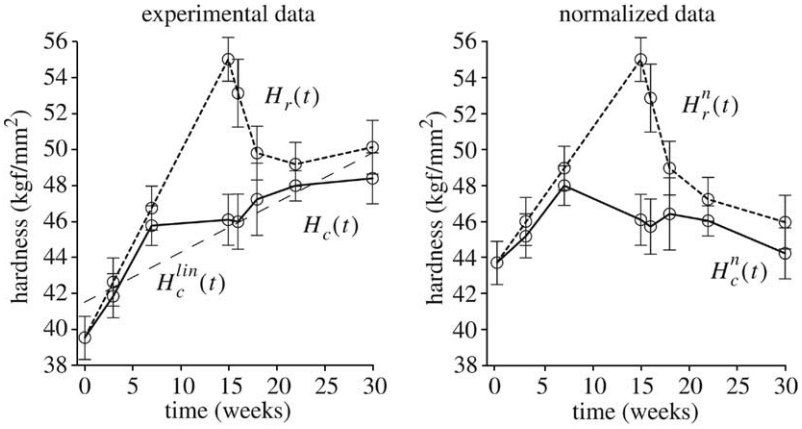

Fig. 3. Experimental hardness measurements (left) and transformed hardness (right), for control (solid) and running group (dotted), during the all experiment period. Each data point represents a mean value over 300 measurements. The linear fit of the control data $\overline{H}$ is represented by a broken line.

added to $\Delta H(t_i)$. Finally, the growth effect was removed in both groups by the following transformations:

$$\begin{aligned}\widetilde{H}_c(t_i) &= H_c(t_i) - \Delta H(t_i) + \overline{H}(t = 15 \text{ weeks}),\\ \widetilde{H}_r(t_i) &= H_r(t_i) - \Delta H(t_i) + \overline{H}(t = 15 \text{ weeks}),\end{aligned} \tag{13}$$

which are graphically represented in Fig. 3.

To derive relative density ϕ from hardness, a relationship between hardness and micro-CT measurements was first obtained, and then completed by a calibration of the micro-CT with hydroxyapatite phantoms. CT number and hardness were locally measured, one after the other, at different locations distributed over the same bone surface used for the previous hardness measurements. A linear relationship was adjusted to these measurements ($r^2 = 0.826$). The calibration of the micro-CT with phantoms of different density values gave another linear relationship between CT and density ρ ($r^2 = 0.999$). Finally, using the definition of ϕ, the following relationship was obtained,

$$\phi = \frac{H + 22.9}{136.7}. \tag{14}$$

The above relation was used to transform all mean hardness measurements to mean relative density values, which were used to determine the unknown parameters of the theoretical model.

4. Parameters identification

Assuming the form of the mechanical stimulus ψ, the theoretical model contained formally six unknown parameters: the densification and resorption rates (v_d, v_r), the response delay for densification and resorption (τ_d, τ_r), and finally the densification and resorption limit of the equilibrium zone (ψ_d, ψ_r). Since these parameters are in fact associated to two distinct processes, there were actually two set of three parameters: v_d, τ_d, ψ_d for densification and v_r, τ_r, ψ_r for resorption. These two sets of parameters were identified separately, one after the other, with the data of the running (densification) period and with data of the return to control (resorption) period.

However, in practice, there were more than six unknowns to be set, in order to identify univocally the model to the experimental data: first the geometry of the bone sample used for hardness test, second, the initial conditions, which were the initial relative density ϕ_0

and the initial value of the integral stimulus ψ_0, third, the elastic e_i and plastic p_i constants used to get the stress $\mathbf{S}$ and the function Y, and finally the external applied forces, which were required in the mechanical equilibrium equations.

Since the bone sample was located at the midshaft of the tibial diaphysis, its geometry was modelled by a hollow cylinder, whose dimensions were derived from average values of micro-CT measurements of the experimental samples (Fujie et al., 2004). The initial density ϕ_0 was simply derived from the initial hardness measurements, and assumed to be uniform in the hollow cylinder. Assuming that bone was in equilibrium before the experiment ($t < 0$), and according to (10) the initial stimulus ψ_0 was equal to its initial value Y_0, which could be calculated from the initial relative density ϕ_0, the initial stress $S_{0-} = S$ ($t < 0$), and the equation of mechanical equilibrium. Finite elements tests, based on precise geometric reconstructions of the bone samples, were performed and compared to experimental compression tests to validate the assumption that elastic, and by the way, plastic constants of the rat tibia were similar to human tibia, which were taken from the literature (Cowin et al., 1987). The external forces were simplified to a pure axial load applied to the hollow homogeneous cylinder. Finally, only two extra-unknowns remained: the axial stress, which was assumed constant and homogeneous, but obviously different for the densification (S_d) and resorption ($S_r = S_{0-}$) process.

Two more unknowns could be eliminated. For the densification process, assuming that the value of ψ_d corresponds to 1000 microstrains (Forwood and Turner, 1995), ψ_d was derived from (5), reducing the unknowns to: v_d, τ_d and S_d. For the resorption process, the equivalent axial stress S_r could be derived from the remodelling Eq. (12), since it corresponded to the equilibrium stress maintaining a constant density value ($\widetilde{Y}(S_r)\phi_0^4 - \psi_d$). Finally, the unknowns of the resorption process were: v_r, τ_r, and ψ_r. The remaining unknown parameters of the model were obtained by a least square error minimization between experimental and predicted values of relative density evolution, which were calculated using standard numerical solving techniques.

5. Results

The results consist in the value of the model's parameters (Table 1), and the corresponding predictions of density evolution during the two periods (Fig. 4). As reported in Table 1, the densification rate v_d was more than 10 times smaller than the resorption rate v_r. The delay for densification τ_d was more than 10 times longer than that the delay for resorption τ_r, which was almost negligible. Using the same conversion to get ψ_d from 1000 microstrains, the resorption limit ψ_r corresponded to 940 microstrains. The effect of the delay can be observed in Fig. 4: during the running period, the maximum densification rate does not occur immediately, but only after some delay (≈2 weeks), whereas for the rest period, the resorption was maximal immediately after the stress change, and then decreased and stabilized. The left part of Fig. 4 shows clearly that the simulated density evolution lies very close to the experimental measurements. The right part of the figure shows the model's prediction beyond the period of the experiment. The solid curve revealed that, at the end of the rest period, resorption was over and density reached an equilibrium value, above the initial one. The dotted curve, which represents the evolution of density if the running activity would have been continued indefinitely, predicted that a remodelling equilibrium would have occurred after about one year.

Table 1
Value of the model's parameters, identified by a least square error minimization of experimental measurements

v_d [w^{-1}]	τ_d [w]	ψ_d [10^{-3}]	S_d [MPa]
0.7 (0.3)	1.9 (0.4)	7.5	9.2 (2.2)
v_r [w^{-1}]	τ_r [w]	ψ_r [10^{-3}]	S_r [MPa]
9.4 (4.0)	0.1 (0.1)	6.6 (0.3)	5.9 (0.2)

Values in parenthesis correspond to the extension of the parameter's value that maintains the predicted density evolution within the standard deviation of the experimental data. For scale, w means week.

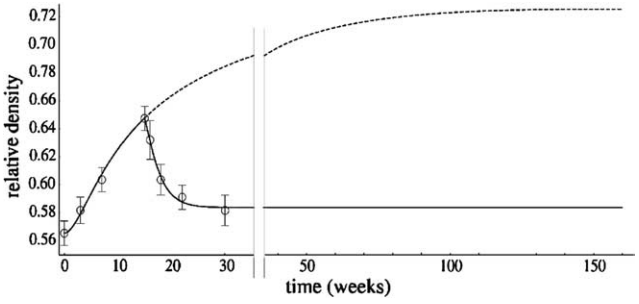

Fig. 4. Relative density evolution (solid line) that best fits the experimental data. The dotted line shows simulated density evolution if the running program was continued indefinitely after the 15th week.

6. Discussion

Bone remodelling includes biological processes such as bone cellular proliferation, differentiation, and mineralization. Remodelling of intracortical bone is specifically indicated by the tissue porosity evolution and microcrack nucleation, which is reflected by osteocyte activities (Verborgt et al., 2000). The intracortical remodelling includes slight porosity change and more (de)mineralization process compared to the trabecular bone adaptation. Instead of porosity, hardness was

therefore chosen for capturing the bone remodelling since the intracortical remodelling involved only very small changes of tissue porosity, which however greatly influence the cortical bone strengths (Martin, 1984; Hayashi et al., 1999).

Several inherent shortcomings in this work may have influenced our results. Among them, we may question about hardness-density relationship, the method for removing growth effects, the validity of the theoretical model, and the choice of upper limit of the equilibrium zone ψ_d.

The relationship between hardness and relative density was only valid in the hardness range (35–65 kg f/mm^2) that was used to get the CT-hardness relationship. Outside this range, the relationship may not be linear. However, since bone hardness in the control and running groups were all within this range, this approximation was applicable for the present analysis.

To isolate the growth effect from the adaptation effect, the simplest transformation was chosen. As an alternative, the hardness could have been normalized by the body weight, which was also measured during the all experiment. However, this would have created another variable (hardness/body weight), which would have been more difficult to link to the relative density. More complex (non-linear) transformations were also tested, but did not significantly changed the results (Terrier, 1999).

The choice of mechanical stimulus has been a long debate, although different stimuli shapes have lead to approximately the same bone remodelling pattern, in experimental (Brown et al., 1990) or numerical (Terrier et al., 1997a,b) studies. Basically, two concepts have been proposed for defining the mechanical stimulus: the strain/stress based theory (Rubin and Lanyon, 1985) and the microcracking theory (Burr et al., 1985). In vivo experiments of the 1980s have shown the role of strain environment in the remodelling process (Rubin and Lanyon, 1985). In the present work, mainly devoted to intracortical remodelling, these two concepts could be however merged into one. Indeed, any strain level can be associated to the occurrence of microcrack of cortical bone even at low strain magnitude (Burr et al., 1985).

For the cortical bone, the distribution of microcracks seems to better directly related to represent the tissue remodelling. The pattern microcracking of young cortical bone corresponds to the distribution of anisotropic plastic yield stress function (Zioupos et al., 1995). For the intracortical bone, bone microcracking was shown to induce osteocyte apoptosis, followed by the resorption phase by osteoclasts, located in the same regions as the regions of osteocyte apoptosis (Verborgt et al., 2000).

Therefore, the direct relation between microcracking, osteocyte death, and initiation of harvesian remodelling supports the idea that a yield stress function is a good candidate for the remodelling stimulus for the intracortical bone. Since bone anisotropy is particularly important for calculating the yield stress function and accounting for the orientation of the microcrack nucleation in the intracortical bone (Jepsen et al., 1999), it was important to account for it in the yield stress function.

To describe the bone elasticity and to calculate the stimulus from stress, five elastic coefficients and five plastic coefficients were required (Rakotomanana et al., 1992). Since the elastic coefficients for the rat tibia were unknown, the values for the human tibia (Cowin, 1989) were used instead, assuming that basic bone contents were the same in rats as well as in humans. The validity of this assumption was confirmed by comparing compression tests of bone samples of rat tibia (Hayashi et al., 1999) with finite element analyses of the same samples using the human elastic coefficients (Terrier, 1999).

Empirical formulae have been extensively developed to relate intracortical relative density to the elastic coefficients and stress strengths of cortical bone through power laws. The power values range from 2.3 (Carter and Hayes, 1977), 5.74 (Currey, 1988) to 10.9 (Schaffler and Burr, 1988). The discrepancy of these results pointed out that the elasticity values became extremely sensitive to the change of porosity when porosity was near zero, which was the case for cortical bone. This justifies the choice of hardness as measured variable, which is not such as sensitive to error as porosity measurement. In the present study, we used a quadratic power law. This choice did not influence the model's parameters since the range of porosity effectively used in the present study was very narrow.

In the present work, we assumed that the "densification stimulus" threshold ψ_d corresponded to 1000 microstrains. In a previous four-point bending model, it has been shown that lamellar bone formation on the endocortical surface of the rat tibiae increases linearly when a threshold of approximately 1000 microstrains is reached (Forwood and Turner, 1995). Although this cannot be directly related to intracortical remodelling, we nevertheless retain this value. This choice was also supported by a similar study using the turkey osteotomy model (Rubin and Lanyon, 1984), which showed that strain below 1000 microstrains is associated to endosteal resorption and intracortical demineralization, whereas strain greater than 1000 microstrains is associated with increased periostal expansion with osteonal remodelling. In other words, a bone reaction was noticed intracortically when the strain exceeded the 1000 microstrains threshold. A sensitivity analysis of the remodelling parameters with respect to ψ_d did not show significant variations. However, further studies on this upper limit should be performed in the future.

A pure axial compression was applied to the midshaft bone sample, while some bending is probably

superposed to the compression. This simplification was however reasonable since the hardness measurements were not significantly different at the different locations (anterior, posterior, medial, lateral), also justifying the averaging of the hardness over the entire surface. Moreover, when the identification procedure was applied separately on each location, we only get a small difference (4%) in the applied stress to fit the experimental data.

The main purpose of this study was to quantify the delay of intracortical remodelling following a stress change. Two stress changes were considered: first, from normal to running activity (inducing densification), and second, from running to normal activity (inducing resorption). To this end, the proposed model implicitly assumed that the primary function of intracortical remodelling is to repair cortical bone microcracks. This assumption was supported by a cause-to-effect relationship between microcracks and Bone Modelling Unit (BMU) activities in cortical bone (Mori and Burr, 1993). However, the amount of time required to repair a microcrack is not clearly defined up to now. We found a densification delay 10 times greater than the resorption delay. This result can by interpreted through the role of osteocyte activities. Delay of three to four days reflects the time required for communication of mechanical signal to osteoprogenitor cells and their differentiation into active osteoblasts (Turner et al., 1998). Other experimental studies have reported that a period of four to five days is necessary after a mechanical stimulus before bone formation begins (Vico and Alexandre, 1989; Ulivieri et al., 1990; Turner and Forwood, 1994; Turner et al., 1998; Verborgt et al., 2000). During an in vivo experiment of rats, it was observed that a single four-point bending (2000 microstrains, 36 cycles at 2 Hz) increased the length of periosteum covered with osteoblasts as early as day 2, with a peak at day 3, and a return to non-loaded levels by day 9 (Boppart et al., 1998). This seems to correspond to a lapse of time required for ''forgetting'' of the initial single session load. On the other side, a delay of nine days could also be attributed to the conversion of osteoblasts to osteocytes and the mineralization of the osteoid (Jaworski and Hooper, 1980). In the same way, ''mineralization lag time'' was normally 10 days (Parfitt, 1983). The small resorption delay observed at the end of the running period was probably enhanced by the effects of unrepaired microcracks routinely generated by running activities. Large amount of microcracks have been shown to induce changes in osteocyte integrity and canaliculi network and then enhance the intracortical bone resorption (Bentolila et al., 1998). These above experiments on cells are consistent with the results obtained here at the tissue level. However, extrapolation of the model's parameters to other bone location should be undertaken with caution. Indeed, it was measured that treadmill exercise of young rat stimulates more their tibia than their lumbar vertebra (Iwamoto et al., 1999).

The densification rate v_d was about 10 times lower than the resorption rate v_r. Extrapolation to humans is not straightforward (load pattern of the quadrupedal rats is very different from that of humans). The ratio v_r/v_d was reported to be about 4 for humans (Nauenberg et al., 1993). The resorption rate v_r obtained for the rat tibia was more than two times higher compared to the one obtained for the human tibia (Terrier, 1999). Moreover, the value of τ_r obtained here for the rats was more then 10 times lower than the one obtained with the same theory from human clinical data on the tibia (Ulivieri et al., 1990). These findings are consistent with previous studies (see review of Cowin, 1989) that lead to the conclusion that adaptation gets faster as mammals become smaller.

In conclusion, by combining theoretical and experimental investigations, we obtained four important parameters of the intracortical bone remodelling for young rats tibiae: the resorption and densification rates, and the delays of resorption and densification. Therefore, this work could not only explain most of the recent results on bone adaptation, but also improved our knowledge of the phenomenon. In particular, the bone response delay was found to be negligibly small for resorption, but significant for densification. This information is critical for the design of protocols to obtain recovery of musculoskeletal tissues after prolonged disuse. However, extrapolation of the experimental data from this work to humans should be undertaken with great caution.

Acknowledgments

This research work was financially supported in part by: (1) The Grand-in-Aid for Monbusko International Scientific Research Program: Joint Research (no. 08044147) from the Ministry of Education, Science and Culture, Japan. (2) The Orthopaedic Hospital of Lausanne, Switzerland.

References

Beaupre, G.S., Orr, T.E., Carter, D.R., 1990. An approach for time-dependent bone modeling and remodeling—theoretical development. J. Orthop. Res. 8, 651–661.

Bennell, K., Page, C., Khan, K., Warmington, S., Plant, D., Thomas, D., Palamara, J., Williams, D., Wark, J.D., 2000. Effects of resistance training on bone parameters in young and mature rats. Clin. Exp. Pharmacol. Physiol. 27, 88–94.

Bentolila, V., Boyce, T.M., Fyhrie, D.P., Drumb, R., Skerry, T.M., Schaffler, M.B., 1998. Intracortical remodeling in adult rat long bones after fatigue loading. Bone 23, 275–281.

Boppart, M.D., Kimmel, D.B., Yee, J.A., Cullen, D.M., 1998. Time course of osteoblast appearance after in vivo mechanical loading. Bone 23, 409–415.

Bourrin, S., Palle, S., Pupier, R., Vico, L., Alexandre, C., 1995. Effect of physical training on bone adaptation in three zones of the rat tibia. J. Bone. Miner. Res. 10, 1745–1752.

Brown, T.D., Pedersen, D.R., Gray, M.L., Brand, R.A., Rubin, C.T., 1990. Toward an identification of mechanical parameters initiating periosteal remodeling: a combined experimental and analytic approach. J. Biomech. 23, 893–905.

Burr, D.B., Martin, R.B., Schaffler, M.B., Radin, E.L., 1985. Bone remodeling in response to in vivo fatigue microdamage. J. Biomech. 18, 189–200.

Carter, D.R., Hayes, W.C., 1977. The compressive behavior of bone as a two-phase porous structure. J. Bone Joint Surg. Am. 59, 954–962.

Cowin, S.C., 1986. Wolff's law of trabecular architecture at remodeling equilibrium. J. Biomech. Eng. 108, 83–88.

Cowin, S.C., 1989. Bone Mechanics. CRC Press, Boca Raton, FL.

Cowin, S.C., Van Buskirk, W.C., Ashman, R.B., 1987. Properties of bone. In: Skalak, R., Chien, S. (Eds.), Handbook of Bioengineering. McGraw-Hill, New York.

Currey, J.D., 1988. The effect of porosity and mineral content on the Young's modulus of elasticity of compact bone. J. Biomech. 21, 131–139.

Eliakim, A., Raisz, L.G., Brasel, J.A., Cooper, D.M., 1997. Evidence for increased bone formation following a brief endurance-type training intervention in adolescent males. J. Bone Miner. Res. 12, 1708–1713.

Forwood, M.R., Turner, C.H., 1995. Skeletal adaptations to mechanical usage: results from tibial loading studies in rats. Bone 17, 197S–205S.

Fujie, H., Miyagaki, J., Terrier, A., Rakotomanana, L., Leyvraz, P.F., Hayashi, K., 2004. Detraining effects on the mechanical properties and morphology of rat tibiae. Biomed. Mater. Eng. 14, 219–233.

Hayashi, K., Myagaki, J., Fujie, H., Terrier, A., Rakotomanana, L., Leyvraz, P.-F., 1999. Biomechanical response of bone to activity change from running to sedentary state in the rat. In: ASME Summer Bioengineering Conference, Montana.

Hazelwood, S.J., Bruce Martin, R., Rashid, M.M., Rodrigo, J.J., 2001. A mechanistic model for internal bone remodeling exhibits different dynamic responses in disuse and overload. J. Biomech. 34, 299–308.

Iwamoto, J., Yeh, J.K., Aloia, J.F., 1999. Differential effect of treadmill exercise on three cancellous bone sites in the young growing rat. Bone 24, 163–169.

Jaworski, Z.F., Hooper, C., 1980. Study of cell kinetics within evolving secondary Haversian systems. J. Anat. 131, 91–102.

Jepsen, K.J., Davy, D.T., Krzypow, D.J., 1999. The role of the lamellar interface during torsional yielding of human cortical bone. J. Biomech. 32, 303–310.

Kaneps, A.J., Stover, S.M., Lane, N.E., 1997. Changes in canine cortical and cancellous bone mechanical properties following immobilization and remobilization with exercise. Bone 21, 419–423.

Kiuchi, A., Arai, Y., Katsuta, S., 1998. Detraining effects on bone mass in young male rats. Int. J. Sports Med. 19, 245–249.

Kummer, B.K.F., 1972. Biomechanics of bone: mechanical properties, functional structure, functional adaptation. In: Fung, Y.C. (Ed.), Biomechanics. Prentice Hall, Englewood Cliffs, pp. 237–271.

Levenston, M.E., Beaupre, G.S., Jacobs, C.R., Carter, D.R., 1994. The role of loading memory in bone adaptation simulations. Bone 15, 177–186.

Maeda, H., Kimmel, D.B., Raab, D.M., Lane, N.E., 1993. Musculoskeletal recovery following hindlimb immobilization in adult female rats. Bone 14, 153–159.

Martin, R.B., 1984. Porosity and specific surface of bone. Critical Reviews in Biomedical Engineering 10, 179–222.

Mori, S., Burr, D.B., 1993. Increased intracortical remodeling following fatigue damage. Bone 14, 103–109.

Nauenberg, T., Bouxsein, M.L., Mikic, B., Carter, D.R., 1993. Using clinical data to improve computational bone remodeling theory. In: 39th Meeting Orthop. Res. Soc., San-Francisco.

Parfitt, A.M., 1983. The physiologic and clinical significance of bone histomorphometric data. In: Recker, R.R. (Ed.), Bone Histomorphometry Techniques and Interpretation. CRC Press, Boca Raton, FL, pp. 143–223.

Rakotomanana, L., 2004. A Geometric Approach to Thermomechanics of Dissipating Continua. Birkhauser, Boston.

Rakotomanana, R.L., Leyvraz, P.F., Curnier, A., Heegaard, J.H., Rubin, P.J., 1992. A finite element model for evaluation of tibial prosthesis–bone interface in total knee replacement. J. Biomech. 25, 1413–1424.

Rakotomanana, R.L., Terrier, A., Ramaniraka, N.A., Leyvraz, P.F., 1999. Anchorage of orthopaedic prostheses: influence of bone properties and bone-implant mechanics. In: Synthesis in Biosolid Mechanics. Kluwer Academic Publishers, Dordrecht.

Rubin, C.T., Lanyon, L.E., 1984. Regulation of bone formation by applied dynamic loads. J. Bone Joint Surg. Am. 66, 397–402.

Rubin, C.T., Lanyon, L.E., 1985. Regulation of bone mass by mechanical strain magnitude. Calcified Tissue Int. 37, 411–417.

Rubin, P.J., Rakotomanana, R.L., Leyvraz, P.F., Zysset, P.K., Curnier, A., Heegaard, J.H., 1993. Frictional interface micromotions and anisotropic stress distribution in a femoral total hip component. J. Biomech. 26, 725–739.

Schaffler, M.B., Burr, D.B., 1988. Stiffness of compact bone: effects of porosity and density. J. Biomech. 21, 13–16.

Terrier, A., 1999. Adaptation of bone to mechanical stress: theoretical model, experimental identification and orthopedic applications. Physics Department, Lausanne, Swiss Federal Institute of Technology.

Terrier, A., Rakotomanana, R.L., Leyvraz, P.F., 1997a. Effect of loading history on short term bone adaptation after total hip arthroplasty. Comput. Meth. Biomech. Biomed. Eng. 2, 115–122.

Terrier, A., Rakotomanana, R.L., Ramaniraka, A.N., Leyvraz, P.F., 1997b. Adaptation models of anisotropic bone. Comput. Meth. Biomech. Biomed. Eng. 1, 47–59.

Turner, C.H., Forwood, M.R., 1994. Bone adaptation to mechanical forces in the rat tibia. In: Weinans, O. (Ed.), Bone Structure and Remodeling, vol. 2. World Scientific Publishing, Amsterdam, pp. 65–78.

Turner, C.H., Owan, I., Alvey, T., Hulman, J., Hock, J.M., 1998. Recruitment and proliferative responses of osteoblasts after mechanical loading in vivo determined using sustained-release bromodeoxyuridine. Bone 22, 463–469.

Ulivieri, F.M., Bossi, E., Azzoni, R., Ronzani, C., Trevisan, C., Montesano, A., Ortolani, S., 1990. Quantification by dual photonabsorptiometry of local bone loss after fracture. Clin. Orthop., 291–296.

Verborgt, O., Gibson, G.J., Schaffler, M.B., 2000. Loss of osteocyte integrity in association with microdamage and bone remodeling after fatigue in vivo. J. Bone Miner. Res. 15, 60–67.

Vico, L., Alexandre, C., 1989. Normalisation of bone cellular responses occurs between 7 and 14 days of simulated weightlessness in rats. Physiologist 32, S25–S26.

Vico, L., Lafage-Proust, M.H., Alexandre, C., 1998. Effects of gravitational changes on the bone system in vitro and in vivo. Bone 22, 95S–100S.

Zioupos, P., Currey, J.D., Mirza, M.S., Barton, D.C., 1995. Experimentally determined microcracking around a circular hole in a flat plate of bone: comparison with predicted stresses. Philos. Trans. R Soc. Lond. B Biol. Sci. 347, 383–396.